REPORT

NEUROSCIENCE

Breathing control center neurons that promote arousal in mice

Kevin Yackle,[1]* Lindsay A. Schwarz,[2]† Kaiwen Kam,[3,4] Jordan M. Sorokin,[5] John R. Huguenard,[5] Jack L. Feldman,[3] Liqun Luo,[2] Mark A. Krasnow[1]‡

Slow, controlled breathing has been used for centuries to promote mental calming, and it is used clinically to suppress excessive arousal such as panic attacks. However, the physiological and neural basis of the relationship between breathing and higher-order brain activity is unknown. We found a neuronal subpopulation in the mouse preBötzinger complex (preBötC), the primary breathing rhythm generator, which regulates the balance between calm and arousal behaviors. Conditional, bilateral genetic ablation of the ~175 *Cdh9*/*Dbx1* double-positive preBötC neurons in adult mice left breathing intact but increased calm behaviors and decreased time in aroused states. These neurons project to, synapse on, and positively regulate noradrenergic neurons in the locus coeruleus, a brain center implicated in attention, arousal, and panic that projects throughout the brain.

Although breathing is commonly viewed as a simple autonomous function that sustains life, it has long been known to influence higher-order behavior and thinking (*1*). Slow, controlled breathing is used by practitioners of pranayama yoga and other forms of meditation to promote mental calming and contemplative states, and it is used clinically to suppress excessive arousal and stress such as certain types of panic attacks (*2*, *3*). Although the effect of breathing on behavior and mental state could easily be indirect, there could also be more direct connections and impact of the breathing center on higher-order brain function (*4*), as demonstrated here.

The preBötzinger complex (preBötC) is a cluster of several thousand neurons in the ventrolateral medulla of the murine brain that can autonomously generate respiratory rhythms in explanted brain slices (*5*, *6*), and whose rhythmic activity in vivo initiates breathing by recurrently activating premotor and motor neurons of the respiratory muscles (*5*). The preBötC is not a homogeneous population of neurons but is composed of distinct, though intermingled, neuronal subpopulations (*5*, *7*), one of which is essential for respiratory-rhythm generation (*8*, *9*) and another for sighing (*10*).

To systematically explore the molecular diversity of breathing center neurons, we screened expression patterns of over 19,000 genes in the Euroexpress embryonic day 14.5 (E14.5) mouse hindbrain database (*11*). Cadherin-9 (*Cdh9*) was the gene most selectively expressed in preBötC (Fig. 1A). We constructed a bacterial artificial chromosome (BAC) transgene with the mOrange coding sequence inserted at the *Cdh9* translation start codon (Fig. 1B). Cell counts in early postnatal brains detected 319 ± 130 (n = 6) Cdh9-mOrange–expressing cells in preBötC (Fig. 1C). These cells intermingled with neurons expressing canonical preBötC markers somatostatin (SST) and neurokinin 1 receptor (NK1R) (Fig. 1, D and E, and fig. S1, A to E). Few expressed the markers themselves: 0 out of 43 Cdh9-mOrange+ cells scored were SST+, and 7 out of 179 Cdh9-mOrange+ (4%) were NK1R+. All Cdh9-mOrange–expressing cells coexpressed neuronal marker NEUN (n = 61 cells, Fig. 1F). These Cdh9-mOrange–expressing neurons can be further divided into seven subtypes based on differential expression of transcription factors *Pax2*, *Dach1*, *Lmo4*, *Evx1*, and *Dbx1*. We focused on the ~175 neurons in each preBötC (fig. S1, F to J; ~350 neurons bilaterally) that coexpress the *Dbx1*-lineage marker, the major subpopulation (56%, 165 out of 292 scored Cdh9-mOrange+ cells, were Dbx1-LacZ+) we call *Cdh9*/*Dbx1* neurons (Fig. 1, G to I).

We electrophysiologically recorded 26 mOrange-positive neurons in 15 preBötC slice preparations from Cdh9-mOrange;Dbx1-lacZ double-transgenic postnatal day 0 to 5 (P0 to P5) mice, then post-stained the neurons for β-galactosidase (LacZ) in some preparations to identify recordings of *Cdh9*/*Dbx1* neurons (table S1). We definitively identified five *Cdh9*/*Dbx1* neurons. One showed bursts of action potentials just before or during each preBötC inspiratory burst (Fig. 1J and fig. S2), like most other *Dbx1*-lineage preBötC neurons (*12*). Three other neurons were more broadly active with bursts during some, but not all, preBötC inspiratory bursts (42, 41, and 88% of inspiratory bursts; Fig. 1K and fig. S2), called an "inspiratory-associated" activity pattern. The other neuron showed sporadic activity with no apparent relationship to preBötC inspiratory bursts. Seven of the 15 Cdh9-mOrange neurons whose Dbx1-lacZ expression status was not determined also displayed inspiratory (four neurons) or inspiratory-associated (two neurons) patterns (table S1).

We used intersectional genetics (Cdh9-LOSL-DTR;Dbx1-cre) (Fig. 1, B, M, and N) to express human diphtheria toxin receptor (DTR) only in *Dbx1*-lineage cells that coexpress *Cdh9*, so that *Cdh9*/*Dbx1* neurons could be specifically ablated by intraperitoneal injection of diphtheria toxin. We expected there would be few, if any, cells besides *Cdh9*/*Dbx1* preBötC neurons that express both genes (*11*, *13*). We examined this in two ways. First, we compared mOrange expression in Cdh9-LOSL-DTR and Cdh9-LOSL-DTR;Dbx1-cre transgenic mice by immunostaining serial sections of adult brains. The only regions where Dbx1-cre reduced the number of mOrange-expressing cells were preBötC and inferior colliculus (fig. S3). Co-staining with other markers showed that loss of mOrange in preBötC was specific and complete for *Cdh9*/*Dbx1* neurons and had little or no effect on the six other (*Dbx1*-negative) *Cdh9*-positive preBötC cell types (fig. S4). Second, immunostaining of serial sections of Cdh9-LOSL-DTR;Dbx1-cre adult brains detected DTR expression only in *Cdh9*/*Dbx1* preBötC neurons (Fig. 1M) and the inferior colliculus (fig. S3). Intraperitoneal injection of diphtheria toxin once a day for 3 days eliminated the DTR-expressing cells (Fig. 1N).

We analyzed adult mice several days after ablating *Cdh9*/*Dbx1* neurons. We expected *Cdh9*/*Dbx1* neurons would be essential for breathing and viability because *Dbx1* neurons are essential for breathing in vivo (*8*, *9*) and ablating just 85 random *Dbx1* neurons abolishes preBötC rhythms in vitro (*14*). However, there was no overt effect on viability (three of three scored mice alive >1 year after ablation), breathing, or sensory and motor behaviors. Plethysmography of freely moving adult mice after ablation did not detect significant differences in inspiratory time, expiratory time, or tidal volume of standard (eupneic) breaths (figs. S5A and S6). No differences were detected in characteristics of four variant breath types (figs. S5, B to E, and S6) or breaths during sleep or under hypercapnic or hypoxic conditions (figs. S5, F to H, and S6).

There was, however, a change in abundance of different breath types, first noted in respiratory-rate histograms: *Cdh9*/*Dbx1* ablation shifted the distribution toward slower breaths (low respiratory rate) (Fig. 2B). Inspection of plethysmograph traces indicated that the shift was due to increased slow breaths (eupneic and grooming) associated with calm behaviors and reduction in rapid breaths associated with sniffing and other active behaviors (Fig. 2A and fig. S7).

[1]Howard Hughes Medical Institute, Department of Biochemistry, Stanford University School of Medicine, Stanford, CA 94305, USA. [2]Howard Hughes Medical Institute, Department of Biology, Stanford University, Stanford, CA 94305, USA. [3]Systems Neurobiology Laboratory, Department of Neurobiology, David Geffen School of Medicine, University of California–Los Angeles, Los Angeles, CA 90095, USA. [4]Department of Cell Biology and Anatomy, Chicago Medical School, Rosalind Franklin University of Medicine and Science, North Chicago, IL 60064, USA. [5]Department of Neurology and Neurological Sciences, Stanford University, Stanford, CA 94305, USA.
*Present address: Department of Physiology, University of California–San Francisco, San Francisco, CA 94158, USA.
†Present address: Department of Developmental Neurobiology, St. Jude Children's Research Hospital, Memphis, TN 38105, USA.
‡Corresponding author. Email: krasnow@stanford.edu

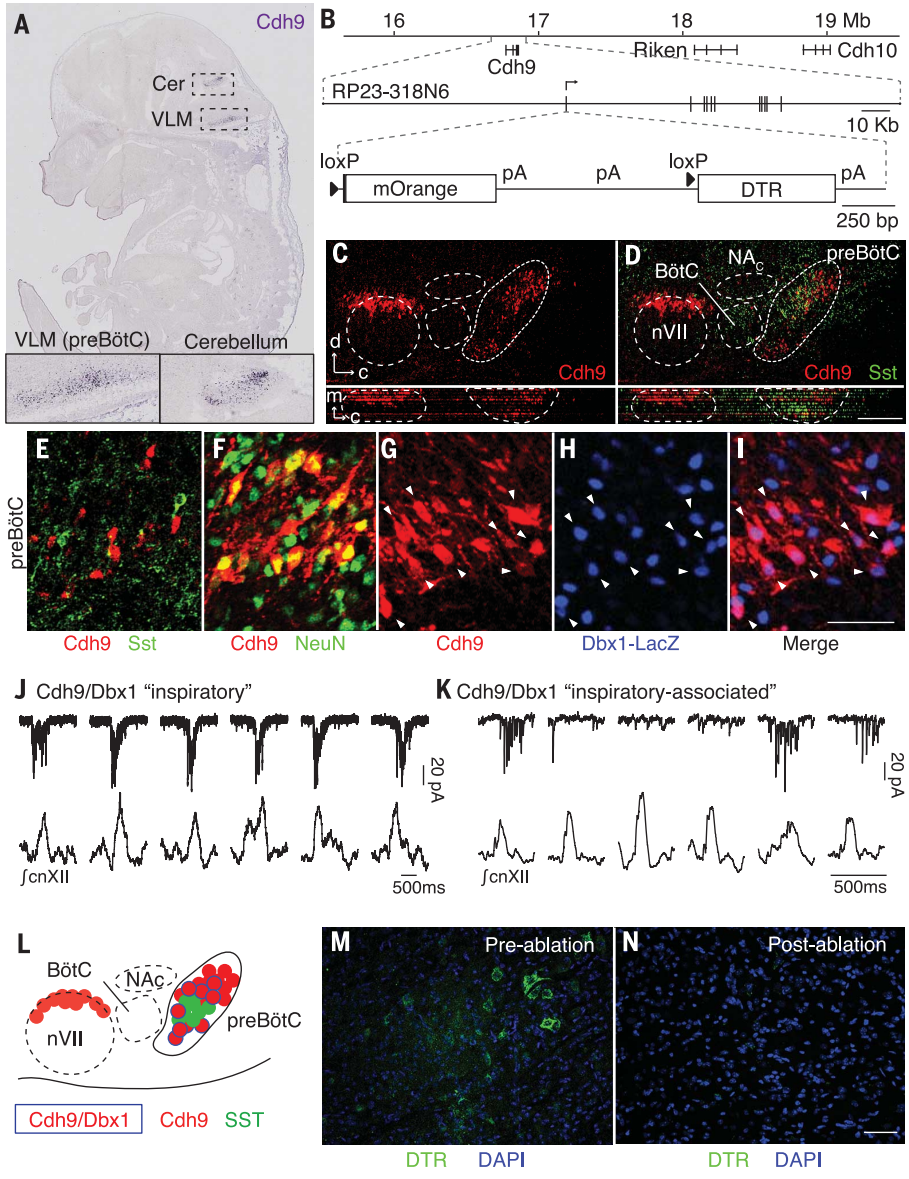

Fig. 1. Identification and genetic ablation of *Cdh9/Dbx1* double-positive neurons in preBötC. (**A**) *Cdh9* mRNA expression (blue) in section of E14.5 mouse embryo (*11*). Insets, ventrolateral medulla (VLM) and ventral cerebellum (Cer). (**B**) (Top) *Cdh9* locus on Chromosome 15 (numbers indicate distance from centromere). (Middle) BAC RP23-318N6. Vertical lines indicate *Cdh9* exons. (Bottom) Cdh9-LOSL-DTR BAC transgene: insertion at *Cdh9* start codon of mOrange sequence and polyadenylation (pA) signals, flanked by *loxP* sites (triangles), followed by DTR sequence. (**C** and **D**) VLM sections of P0 Cdh9-LOSL-DTR mouse immunostained for mOrange to show *Cdh9* expression (red) and P0 wild-type mouse immunostained for somatostatin (SST, green), shown aligned [registered by compact nucleus ambiguus (NA_C), cranial nerve 7 (nVII), and ventral brainstem surface] in sagittal plane (upper panels) and transverse projection (lower panels). d, dorsal; c, caudal; m, medial. Scale bar, 200 μm. (**E** to **I**) preBötC of a P0 Cdh9-LOSL-DTR [(E) and (F)] or Cdh9-LOSL-DTR;Dbx1-lacZ [(G) to (I)] mouse immunostained for Cdh9-mOrange [(E) to (G) and (I), red], SST [(E), green], NEUN [(F), green], or β-galactosidase [*Dbx1*-LacZ, (H) and (I), blue]. Among *Cdh9*-expressing neurons, none coexpressed SST (n = 43 cells), all coexpressed NEUN (n = 57), and 56% coexpressed *Dbx1* reporter (n = 292, arrowheads). Scale bar [(E) to (I)], 50 μm. (**J** and **K**) Whole-cell voltage-clamp recordings of *Cdh9/Dbx1* preBötC neurons in slice *Cdh9* preparations (top) and simultaneous integrated cranial nerve 12 (cnXII) activity (bottom). Neuron in (J) (neuron 1, table S1) shows bursts in all inspiratory events (inspiratory pattern). Neuron in (K) (neuron 3) shows more widespread activity but bursts only during some events (inspiratory-associated). Scale bars, 500 ms. (**L**) Schematic of VLM. *Cdh9/Dbx1* neurons (blue border) intermingle with SST (green) and other *Cdh9* neurons (red) in preBötC. (**M** and **N**) Intersectional genetic labeling of *Cdh9/Dbx1* preBötC neurons with DTR (immunostain, green) in ~P35 Cdh9-LOSL-DTR;Dbx1-cre mice before (M) and after (N) intraperitoneal DT injection to ablate them. Scale bar, 50 μm.

The change in breathing patterns after *Cdh9/Dbx1* neural ablation was accompanied by a corresponding change in behavior. Ablation reduced exploration of a new environment (87 ± 9% versus 62 ± 20% time spent in active exploration, pre- versus postablation; P = 0.02) and increased time engaged in grooming threefold (10 ± 7% versus 31 ± 16%; P = 0.02) and still-sitting twofold (3 ± 4% versus 7 ± 7%; P = 0.07), although the latter did not reach statistical significance (Fig. 2C). There was an increase in both number of calm episodes (Fig. 2D) and their duration (Fig. 2E and movie S1). Because the breathing pattern associated with each behavioral state was not detectably altered by ablation (figs. S5 and S6), the observed change in respiratory-rate distribution could be explained by the overall change in behavior (fig. S8): a shift from active toward calm behaviors. Electrocorticographic (ECoG) monitoring showed an increase in slow-wave (delta, 2 to 4 Hz) brain activity after ablation (Fig. 2F) and a selective decline in time spent in an active-brain state dominated by theta activity (Fig. 2G) compared to that of littermate controls (Fig. 2, H and I). These changes could be temporarily reversed by illuminating the chamber, providing a stimulus that apparently overrides the decrease in arousal caused by *Cdh9/Dbx1* ablation (fig. S9).

To confirm that the observed behavioral and breathing changes were due to ablation of neurons in the preBötC, we restricted DTR induction and hence neural ablation to just *Cdh9*-expressing preBötC neurons (fig. S10, A to C). The animals displayed a diminution in active exploratory behaviors and breathing patterns and an increase in calm behaviors and breathing patterns similar to animals with *Cdh9/Dbx1* neurons ablated using our intersectional genetic strategy (compare fig. S10, D and E, and Fig. 2).

The decrease in active behavior and increase in ECoG delta waves observed after *Cdh9/Dbx1* neuron ablation is reminiscent of changes following silencing or ablation of the locus coeruleus (LC), a noradrenergic nucleus in the pons implicated in generalized arousal, stress, and sleep-wake transitions (*15*). We thus microinjected two retrograde tracers into the LC and found that both labeled Cdh9-mOrange neurons in preBötC (FluorGold: fig. S11, A to C; fluorescent retrograde beads: data not shown). Most of the labeled Cdh9-mOrange preBötC neurons (85%, 23 out of 27, n = 40 sections, 3 mice) were contralateral to the injection site. The connection is selective because most labeled preBötC neurons expressed Cdh9-mOrange (72%, 13 out of 18, n = 10 sections, 4 mice), and no retrograde labeling of Cdh9-mOrange neurons was observed following tracer injection into regions surrounding the LC (n = 4 injections).

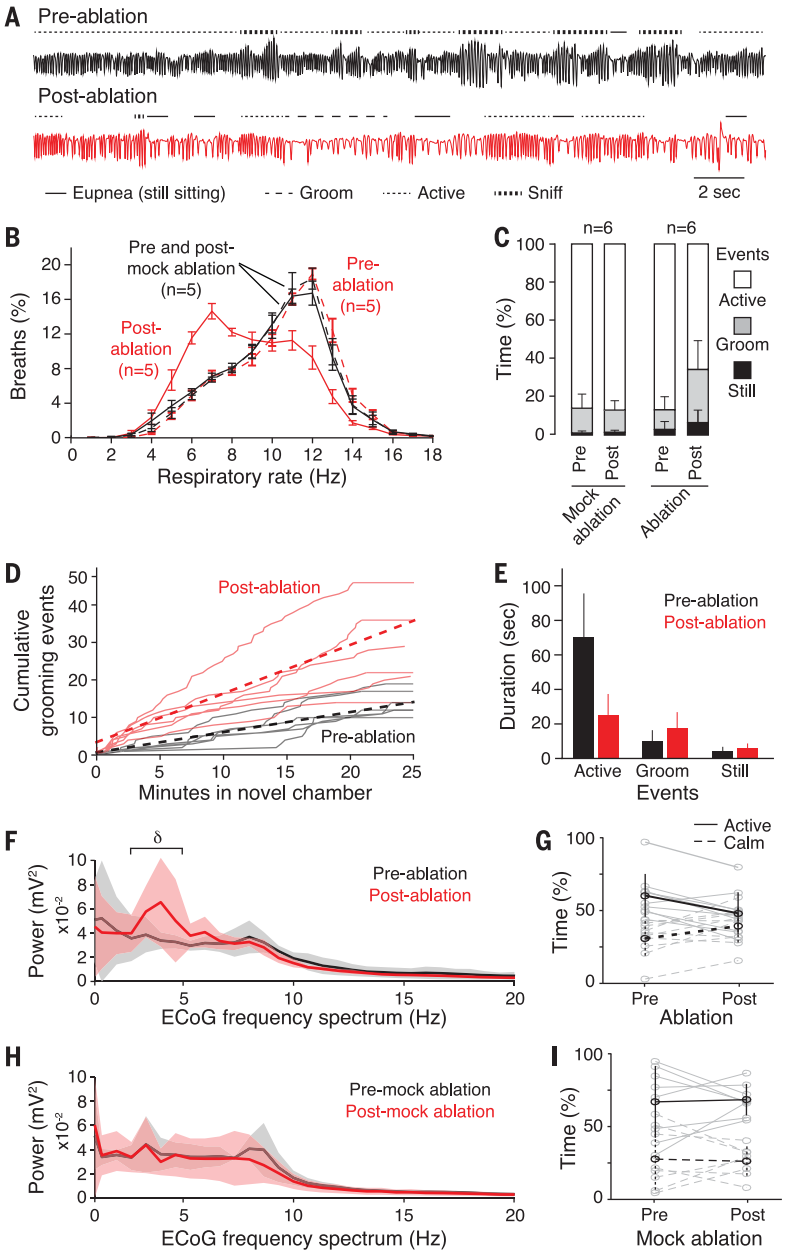

Fig. 2. Respiratory and behavior changes after *Cdh9/Dbx1* neuron ablation. (**A**) Plethysmography airflow traces of Cdh9-LOSL-DTR;Dbx1-cre mice before (black) and 2 days after (red) *Cdh9/Dbx1* ablation. Note increased grooming and eupneic breaths and decreased active breaths and sniffing after ablation (see key). Scale bar, 2 s. (**B**) Distribution of respiratory rates (bin size 1 Hz) in 40-min assay of control (wild-type, Cdh9-LOSL-DTR, or Dbx1-cre; black, n = 5) and experimental (Cdh9-LOSL-DTR; Dbx1-cre; red, n = 5) animals before (dashed lines) and 2 days after (solid lines) *Cdh9/Dbx1* ablation. (**C**) Percent of time in plethysmography chamber spent still-sitting (black), grooming (gray), or active (white) by control (n = 6) or experimental (n = 6) mice before (pre) or 2 days after (post) ablation or mock ablation. P values comparing pre- and postablation behavior: active (0.02), grooming (0.02), and still-sitting (0.07). (**D**) Grooming events in new chamber of Cdh9-LOSL-DTR;Dbx1-cre mice before (black) or after (red) ablation. Solid lines, individual mice (n = 6); dashed lines, average. (**E**) Duration of behaviors in (C) (mean ± SD, n = 6). After ablation, active episodes shortened (P = 0.005), grooming and still-sitting showed nonsignificant trend to lengthening (P = 0.24 and 0.21, respectively). (**F** and **H**) ECoG power spectral analysis [average (solid lines) ± SEM] of 20-min recording (trial 1) of Cdh9-LOSL-DTR;Dbx1-cre [(F), n = 5] or control Cdh9-LOSL-DTR [(H), n = 4] mice before (black) or 4 to 10 days after (red) ablation. δ, delta wave; V, voltage. Active behavior correlates with faster breathing (fig. S15, C to E). (**G** and **I**) Time spent in active (solid black line, mean ± SEM) and calm (dashed black line) behavioral states defined by electromyography (EMG) and ECoG (fig. S15) of individual animals in (F) and (H) (gray lines) during two 20-min assays pre- and post-*Cdh9/Dbx1* ablation. Note decreased active and increased calm periods following ablation in experimental animals (P = 0.001 and 0.02, respectively, paired t test) and no change in controls (P = 0.86 and 0.81, respectively).

We tested whether the observed connection between the preBötC neurons and LC is direct to the noradrenergic [dopamine β-hydroxylase (*Dbh*)–expressing] neurons that dominate the LC (*15*). Injection of Cre-dependent adeno-associated virus (AAV) helper viruses (AAV-FLEx^{loxP}-TVA: mCherry and AAV-FLEx^{loxP}-rabies glycoprotein), which enables infection and monosynaptic spread of an envA-pseudotyped, glycoprotein-deleted, and GFP-expressing rabies virus (RVdG) (*16*), into the LC of Dbh-cre;Cdh9-mOrange mice resulted in specific infection of LC "starter" neurons by RVdG (fig. S12) and selective retrograde transsynaptic tracing (GFP-labeling) of Cdh9-mOrange neurons in the preBötC (Fig. 3, A to D, and fig. S11, D to F). We again observed a strong bias for labeling the contralateral rather than ipsilateral preBötC (compare Fig. 3, A to C, and fig. S11, D to F). Most of the green fluorescent protein (GFP)–labeled neurons in the contralateral preBötC (63%, 45 out of 72, n = 18 sections, 3 mice) expressed Cdh9-mOrange, whereas few of the labeled ipsilateral preBötC neurons expressed Cdh9-mOrange (7%, 7 out of 94, n = 18 sections, 3 mice). Nearly all ipsilateral GFP-expressing neurons were located outside the canonical preBötC region defined by SST expression, so they are presumably not preBötC neurons (fig. S13). Control experiments in mice without Dbh-cre did not show double-positive preBötC neurons (fig. S12).

We microinjected a retrogradely transported *cre*-expressing virus, canine adenovirus type 2–Cre (CAV-Cre), bilaterally into the LC of Cdh9-LOSL-DTR mice to eliminate mOrange and express DTR only in the *Cdh9*-expressing neurons that project to LC (Fig. 3E). Before DT injection, animals breathed and behaved normally, although there was an increase in calm breathing relative to mock-ablated controls, perhaps because of neural toxicity associated with induced DTR expression (Fig. 3, H and I). Four to 10 days after DT injection and ablation of LC-projecting, *Cdh9*-expressing preBötC neurons (Fig. 3, F and G), there was a change in breathing (Fig. 3H) and decrease in active behaviors (Fig. 3I) that mimicked those observed after ablation of the *Cdh9*/*Dbx1* preBötC neurons (compare to Fig. 2, B and C).

We examined LC activity by c-FOS expression (*17*) following *Cdh9*/*Dbx1* neuron ablation. Under standard housing conditions, Cdh9-LOSL-DTR; Dbx1-cre littermate control mice with intact *Cdh9*/*Dbx1* neurons showed only occasional LC activity (Fig. 4, A and D, and fig. S14). When animals were placed in a new environment (plethysmography

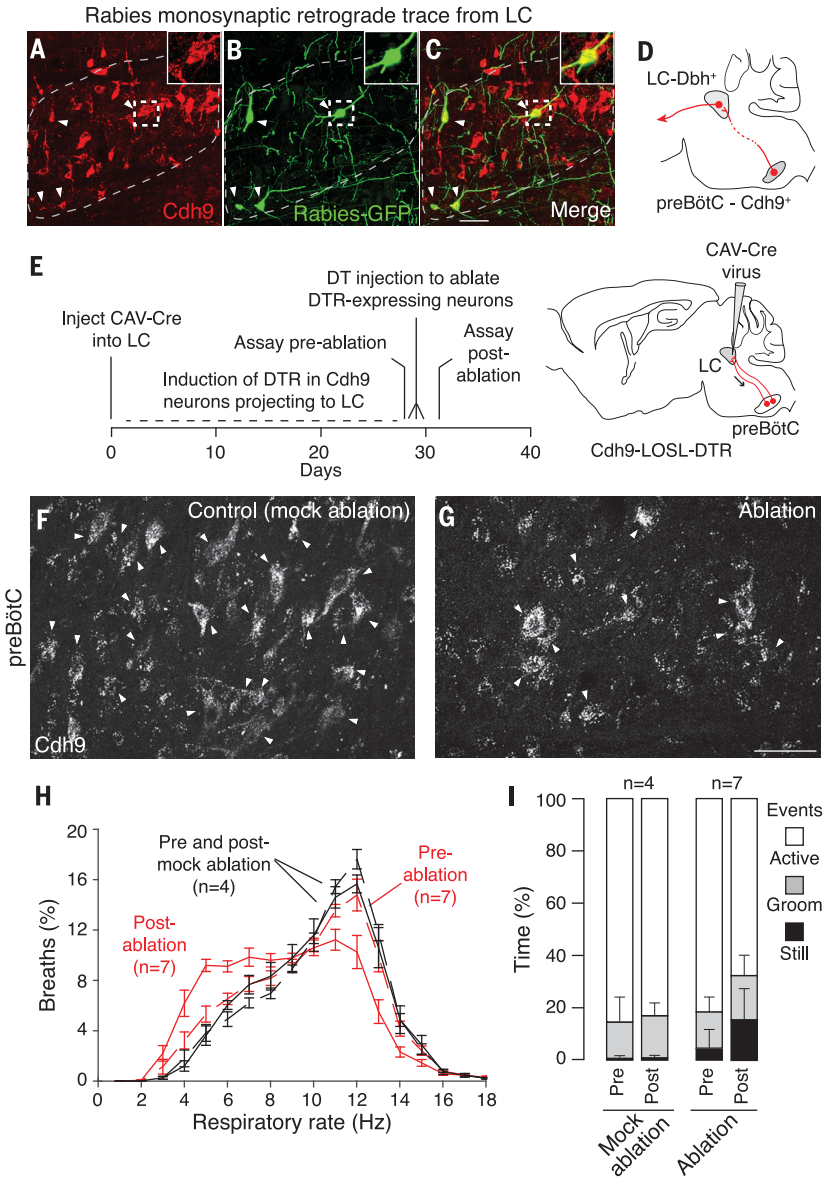

Fig. 3. Effect on breathing and behavior of ablation of *Cdh9* neurons that project to and synapse on LC neurons. (**A** to **D**) Rabies virus monosynaptic retrograde trace from dopamine β-hydroxylase (*Dbh*)–expressing locus coeruleus (LC) neurons. Section through contralateral preBötC (A) to (C) of adult Cdh9-LOSL-DTR;Dbh-cre mouse 5 days after unilateral LC injection of rabies-GFP and helper virus, immunostained to show *Cdh9*-expressing neurons (mOrange, red). Arrowheads indicate colocalization of GFP and mOrange. Insets highlight boxed region. Scale bar, 50 μm. (D) Schematic of monosynaptic projection (red line) from *Cdh9*-expressing preBötC neurons (red circle) to contralateral LC, which projects to higher brain structures (arrow). (**E**) Scheme for ablating only *Cdh9*-expressing preBötC neurons that project to LC. CAV-Cre virus injected bilaterally into LC of adult Cdh9-LOSL-DTR mice (right) is taken up by *Cdh9*-expressing preBötC neurons that project there (red). Cre induces DTR expression, and DT injection induces ablation. (**F** and **G**) preBötC Cdh9-mOrange expression (white) in control uninjected [(F), mock ablation] and CAV-Cre injected [(G), ablation] Cdh9-LOSL-DTR mice 2 days after DT injection. Scale bar, 50 μm. Quantification showed 32% (mean) and 50% (maximal) reduction in mOrange neurons (n = 15 sections), close to the value expected if all *Cdh9/Dbx1* preBötC neurons (50% of *Cdh9*-expressing neurons) project to LC. (**H**) Distribution of respiratory rates in 40-min assay (as in Fig. 2B) of CAV-Cre injected Cdh9-LOSL-DTR adult mice (red, n = 7) or wild-type littermates (black, n = 4) before (dashed) and 2 days after (solid) DT injection. (**I**) Behavioral analysis (as in Fig. 2C) of mice in (H). Pre- versus postablation P values: active (0.015), grooming (0.37), and still-sitting (0.015). The increased calm events in preablation experimental versus control mice was reproducible; it may be due to toxicity of DTR induced in adult neurons, which is not observed in Cdh9-LOSL-DTR;Dbx1-cre mice when DTR is expressed in early development, perhaps due to developmental compensation.

chamber) for 1 hour, c-FOS was induced in scattered cells throughout the LC (Fig. 4, B and D, and fig. S14). However, 4 days after *Cdh9/Dbx1* neuron ablation, only rare c-FOS–positive LC neurons were detected before or after placement in the chamber (Fig. 4, C and D, and fig. S14). The LC of ablated animals remained responsive to the extreme arousal stimulus of physical-restraint stress (*18*) (Fig. 4, D to F, and fig. S13), indicating that other LC inputs and functions were intact.

We have identified and characterized a new neuronal subtype in the preBötC comprising ~175 of its ~3000 neurons. The *Cdh9/Dbx1* neurons are dispensable for respiratory-rhythm generation and instead promote generalized behavioral arousal. Ablation of these neurons left all major breathing patterns and regulation intact but made the mice preternaturally calm: Their activity and ECoG profiles shifted from active exploratory behavior and brain wave patterns toward calm behaviors such as still-sitting and grooming. Monosynaptic tracing demonstrated that these neurons directly project to and synapse on noradrenergic neurons in the contralateral LC, which in turn project throughout the brain and control generalized arousal and sleep-wake transitions (*15*). *Cdh9/Dbx1* preBötC neurons provide excitatory input to the LC and appear to be the dominant activating input under mild arousal conditions of placement in a new chamber.

We propose that *Cdh9/Dbx1* preBötC neurons function as gateway neurons directly linking the preBötC to the locus coeruleus, and through it to the rest of the brain (Fig. 4G). This ascending circuit allows the respiratory center to communicate directly with and control higher-order brain structures associated with behavioral arousal. The excitatory input to the LC is presumably provided by the observed inspiratory-associated activity patterns of *Cdh9/Dbx1* neurons, which could provide greater excitatory input with faster respiratory rates and perhaps abnormal respiratory patterns (Fig. 4H). This respiratory corollary signal would thus serve to coordinate the animal's state of arousal with the breathing pattern, leaving the animal calm and relaxed when breathing is slow and regular, but promoting (or maintaining) arousal when breathing is rapid or disturbed. This circuit and corollary signal would explain why preBötC respiratory patterns have been observed in the LC and other reticular activating structures (*19*–*21*). The LC can increase respiratory rate (*22*), so there may also be a positive feedback loop from the LC ultimately back to *Cdh9/Dbx1* preBötC neurons.

The *Cdh9/Dbx1* circuit may have evolved as a defense response, mobilizing the animal in the face of rapid, irregular, or labored breathing. Indeed, fast or erratic breathing in humans increases alertness and can cause anxiety and even panic (*3*), and likewise increased preBötC activity, hyperventilation, and sighs appear to induce arousal during sleep (*23*–*25*). Conversely, slow and controlled breathing has long been known by practitioners of

pranayama yoga to induce relaxation, and related approaches have proven useful for anxiety syndromes and other stress disorders (*1*, *2*). If the *Cdh9/Dbx1* circuit is conserved in humans, it could provide a therapeutic target for breathing-related anxiety disorders and perhaps prevention of sudden infant death syndrome (SIDS), widely hypothesized to result from an inadequate arousal response to asphyxiation during sleep (*24*).

Notably, panic attacks triggered by respiratory symptoms are specifically responsive to clonidine, an α2-adrenergic agonist that silences LC (*26*).

Although breathing is generally thought of as an autonomic behavior, higher-order brain functions can exert exquisite control over breathing. Our results show, conversely, that the breathing center has a direct and powerful influence on higher-order brain function. It will thus be important to map the full range of behaviors and functions the breathing center controls.

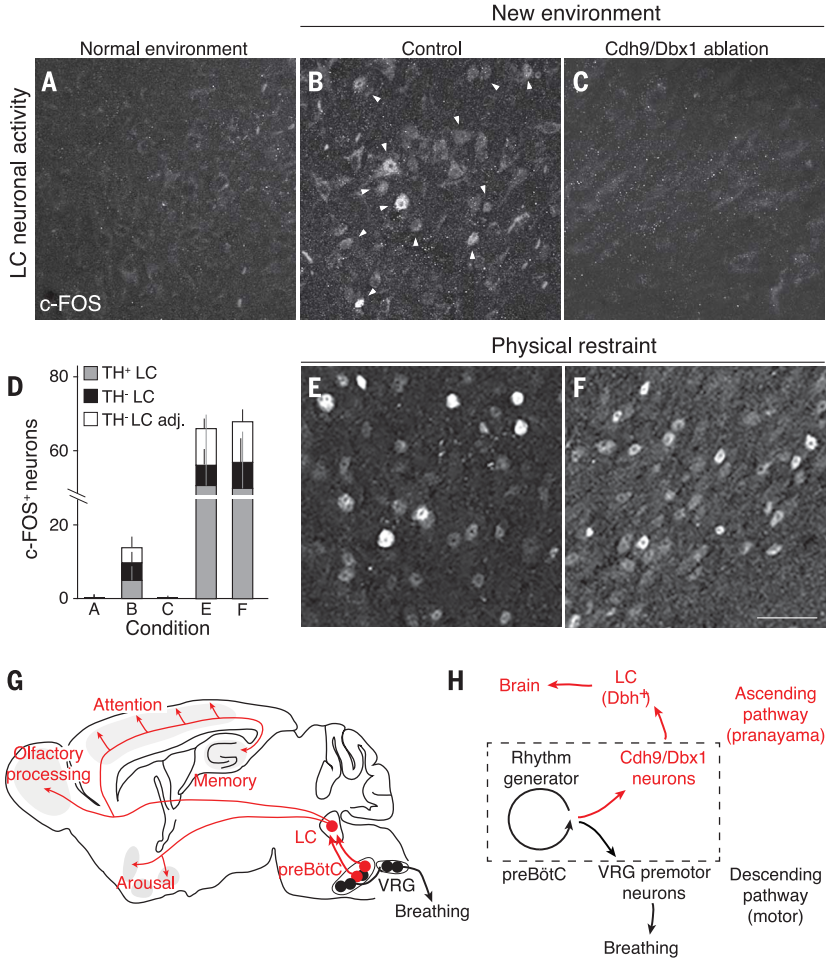

Fig. 4. Effect of *Cdh9/Dbx1* neuron ablation on LC neuronal activity. (**A** to **C**, **E**, and **F**) c-FOS immunostaining (arrowheads) in LC of adult wild-type mouse in normal environment [home cage, (A)] and of control [wild-type, Cdh9-LOSL-DTR, or Dbx1-cre mice, (B) and (E)] and *Cdh9/Dbx1*-ablated mice [Cdh9-LOSL-DTR;Dbx1-cre mice 2 days after DT injection, (C) and (F)] after 1 hour in new chamber [(B) and (C)] or in a conical tube under physical restraint [(E) and (F)]. Scale bar, 50 μm. (**D**) Quantification of c-FOS$^+$ neurons in (A) to (C) and (E) and (F) (mean ± SD) per 25-μm section of LC: (A) 0.4 ± 0.8 neurons (n = 39 sections, 6 animals); (B) 13.8 ± 6.5 neurons (14 sections, 4 animals); (C) 0.1 ± 0.3 neurons (17 sections, 6 animals); (E) 61.4 ± 31.4 neurons (5 sections, 3 animals); and (F) 63.8 ± 19.9 neurons (6 sections, 3 animals). c-FOS$^+$/TH$^+$ neurons, gray; c-FOS$^+$/TH$^-$ neurons embedded within TH$^+$, black; c-FOS$^+$/TH$^-$ neurons directly surrounding TH$^+$ LC region, white. (**G**) Ascending neural circuit from preBötC. *Cdh9/Dbx1* preBötC neurons (red) provide monosynaptic excitatory input to noradrenergic LC neurons (red), which project throughout brain to promote arousal and active behaviors. Also shown is the classical circuit from preBötC rhythm-generating neurons (black) to premotorneurons in ventral respiratory group (VRG, black). (**H**) Model of preBötC with *Cdh9/Dbx1* neurons distinct from, but regulated by, rhythm-generating neurons. This provides an ascending respiratory corollary signal to the LC and on to the rest of the brain, separate from classical descending motor circuit. Hence, when breathing speeds up or is otherwise altered, *Cdh9/Dbx1* neurons activate LC to induce or maintain an aroused state. [Less direct circuits or downstream events from *Cdh9/Dbx1* neurons could also contribute to LC activation, and because LC also regulates sensory modalities (*27*, *28*), sensory alterations could also contribute to LC-induced behaviors. In addition, a direct contribution of *Cdh9/Dbx1* neurons to preBötC breathing-rhythm generation cannot be excluded, because compensatory mechanisms may obscure them.]

REFERENCES AND NOTES

1. R. P. Brown, P. L. Gerbarg, *Ann. N. Y. Acad. Sci.* **1172**, 54–62 (2009).
2. R. P. Brown, P. L. Gerbarg, *J. Altern. Complement. Med.* **11**, 711–717 (2005).
3. A. E. Nardi, R. C. Freire, W. A. Zin, *Respir. Physiol. Neurobiol.* **167**, 133–143 (2009).
4. M. B. Parshall *et al.*, *Am. J. Respir. Crit. Care Med.* **185**, 435–452 (2012).
5. J. L. Feldman, C. A. Del Negro, P. A. Gray, *Annu. Rev. Physiol.* **75**, 423–452 (2013).
6. J. C. Smith, H. H. Ellenberger, K. Ballanyi, D. W. Richter, J. L. Feldman, *Science* **254**, 726–729 (1991).
7. P. A. Gray, J. C. Rekling, C. M. Bocchiaro, J. L. Feldman, *Science* **286**, 1566–1568 (1999).
8. J. Bouvier *et al.*, *Nat. Neurosci.* **13**, 1066–1074 (2010).
9. P. A. Gray *et al.*, *J. Neurosci.* **30**, 14883–14895 (2010).
10. P. Li *et al.*, *Nature* **530**, 293–297 (2016).
11. G. Diez-Roux *et al.*, *PLOS Biol.* **9**, e1000582 (2011).
12. M. C. Picardo, K. T. Weragalaarachchi, V. T. Akins, C. A. Del Negro, *J. Physiol.* **591**, 2687–2703 (2013).
13. A. Pierani *et al.*, *Neuron* **29**, 367–384 (2001).
14. X. Wang *et al.*, *eLife* **3**, e03427 (2014).
15. C. W. Berridge, B. D. Waterhouse, *Brain Res. Brain Res. Rev.* **42**, 33–84 (2003).
16. I. R. Wickersham *et al.*, *Neuron* **53**, 639–647 (2007).
17. M. Sheng, M. E. Greenberg, *Neuron* **4**, 477–485 (1990).
18. J. G. McCall *et al.*, *Neuron* **87**, 605–620 (2015).
19. P. G. Guyenet, N. Koshiya, D. Huangfu, A. J. Verberne, T. A. Riley, *Am. J. Physiol.* **264**, R1035–R1044 (1993).
20. Y. Oyamada, D. Ballantyne, K. Mückenhoff, P. Scheid, *J. Physiol.* **513**, 381–398 (1998).
21. Z. Chen, F. L. Eldridge, P. G. Wagner, *J. Physiol.* **437**, 305–325 (1991).
22. G. Hilaire, J. C. Viemari, P. Coulon, M. Simonneau, M. Bévengut, *Respir. Physiol. Neurobiol.* **143**, 187–197 (2004).
23. K. Gleeson, C. W. Zwillich, *Am. Rev. Respir. Dis.* **145**, 453–457 (1992).
24. H. C. Kinney, B. T. Thach, *N. Engl. J. Med.* **361**, 795–805 (2009).
25. J. M. Ramirez, *Prog. Brain Res.* **209**, 91–129 (2014).
26. A. M. Valença *et al.*, *Arq. Neuropsiquiatr.* **62** (2b), 396–398 (2004).
27. M. Jiang, E. R. Griff, M. Ennis, L. A. Zimmer, M. T. Shipley, *J. Neurosci.* **16**, 6319–6329 (1996).
28. L. Hickey *et al.*, *J. Neurosci.* **34**, 4148–4160 (2014).

ACKNOWLEDGMENTS

K.Y. performed in situ screen; generated and characterized Cdh9 transgene; characterized *Cdh9/Dbx1* neuronal ablation; and performed AAV-Cre, FluoroGold, and retrograde bead injections and c-Fos experiments. L.A.S. and L.L. provided the reagents and L.A.S. injected rabies and CAV-Cre viruses. K.K. and J.L.F. provided the reagents and K.K. performed and analyzed slice electrophysiology. J.M.S. and J.R.H. provided the reagents and J.M.S. performed and analyzed ECoG recording. K.Y. analyzed all data. K.Y. and M.A.K. conceived experiments, interpreted data, and wrote the manuscript. All authors edited the manuscript. We thank X. Chen and G. Nachtrab for assistance and reagents for AAV-Cre injection, J. Zeitzer for assistance with ECoG analysis, and members of the Krasnow lab for helpful comments. This work was supported by the Howard Hughes Medical Institute (M.A.K. and L.L.), NIH grants HL70029 and HL40959 (J.L.F.), and the NIH Medical Scientist Training Program (K.Y.). M.A.K. and L.L. are investigators of the Howard Hughes Medical Institute. Data are curated and stored in the Krasnow lab at the Howard Hughes Medical Institute, Department of Biochemistry, Stanford University School of Medicine, Stanford, CA 94305, USA.

SUPPLEMENTARY MATERIALS

www.sciencemag.org/content/355/6332/1411/suppl/DC1
Materials and Methods
Figs. S1 to S15
Table S1
References (*29*–*46*)
Movie S1

21 August 2016; accepted 1 February 2017
10.1126/science.aai7984

Breathing control center neurons that promote arousal in mice
Kevin Yackle, Lindsay A. Schwarz, Kaiwen Kam, Jordan M. Sorokin, John R. Huguenard, Jack L. Feldman, Liqun Luo and Mark A. Krasnow (March 30, 2017)
Science **355** (6332), 1411-1415. [doi: 10.1126/science.aai7984]

Editor's Summary

The calming effect of breathing

The rhythmic activity of a cluster of neurons in the brainstem initiates breathing. This cluster is composed of distinct, though intermingled, subgroups of neurons. Yackle *et al.* found a small, molecularly defined neuronal subpopulation in this breathing rhythm generator that directly projects to a brain center that plays a key role in generalized alertness, attention, and stress (see the Perspective by Sheikbahaei and Smith). Removal of these cells did not affect normal breathing but left the animals unusually calm. The breathing center thus has a direct and dramatic influence on higher-order brain function.

Science, this issue p. 1411; see also p. 1370